Chapter 11
Non-stationary Dynamics and Coupled Oscillations

Inspired by a presentation of Sanjay Mittal [245, 250, 260] and a discussion with Paolo Galdi (private communication, 2016) we study the interaction of the *von Kármán vortex sheet* with the oscillation of an elastic obstacle. The flow around a blunt body develops self-excited oscillations. Elastic structures freely oscillate with Eigenfrequencies. We want to study the interplay between these two effects on a coupled elastic fluid-structure interaction problem.

Mittal and coworkers [260] studied the interaction of a freely oscillating rigid body in a laminar flow. They considered obstacles with circular and elliptical cross section that are freely suspended and attached to an (imaginary) spring. The solid problem alone—without interaction to a surrounding fluid—will show periodic oscillations of a fixed frequency and amplitude. The amplitude is related to the initial excitation, while the frequency of the oscillation is related to the spring constant and the mass of the obstacle. Second, the rigid obstacle is fixed and one studies the flow of an incompressible fluid around this obstacle. The resulting fluid pattern will strongly depend on key quantities like the Reynolds number

$$Re = \frac{\bar{\mathbf{v}}D}{\nu},$$

where by $\bar{\mathbf{v}}$ we denote the average velocity of the surrounding fluid, by D the diameter of the obstacle and by ν the viscosity of the fluid. Increasing the Reynolds number results in the following observations

- In the *subcritical regime* $Re < Re_{sub}$, the flow has stationary limit with $\partial_t \mathbf{v} = 0$.
- In the *laminar regime* $Re_{sub} < Re < Re_{lam}$, the flow develops an oscillatory pattern behind the obstacle, the so called *von Kármán vortex street*, see [333] or

T. Richter, *Fluid-structure Interactions*, Lecture Notes in Computational Science and Engineering 118, DOI 10.1007/978-3-319-63970-3_11

Fig. 11.3. The frequency f of the oscillation is connected to the *Strouhal number* St, that is like the *Reynolds number* an non-dimensional measure

$$St = \frac{fD}{\bar{\mathbf{v}}},$$

where f is the frequency, D the diameter of the object and $\bar{\mathbf{v}}$ the velocity of the surrounding fluid. For a large range of Reynolds numbers (in the laminar regime), it holds for the flow around circular objects

$$St \approx 0.2\left(1 - \frac{20}{Re}\right) \quad \Leftrightarrow \quad f = 0.2\left(\frac{\bar{\mathbf{v}}}{D} - \frac{20\nu}{D^2}\right), \tag{11.1}$$

showing that the frequency will linearly increase with the velocity.

- In the *transition regime* $Re_{lam} < Re < Re_{trans}$, the flow develops complex patterns. The dominant oscillation of the vortex street is overlayed with more and more overtones.
- Finally, the flow pattern completely changes in the *turbulent regime* for $Re \gg Re_{trans}$, where the motion appears chaotic.

In a series of papers, Mittal [244, 245, 260] analyzed the interaction of the non-stationary vortex street of laminar flows with an rigid, but freely supported obstacle: What is the resulting frequency and what is the resulting amplitude for the dynamically coupled problem? Two of the findings are the following: First, the coupled problem admits non-stationary periodic solutions at significantly reduced Reynolds numbers (as compared to the pure fluid problem). Second, and this effect is referred to as *synchronization* or *lock-in*, there is a region of Reynolds numbers, where the frequency of the coupled system is stable and usually equal or a multiple of the natural structure frequency [33, 297, 349].

Here, we aim at discussion this question for a fully coupled fluid-structure interaction problem with an elastic obstacle. We consider the benchmark problem that has already been introduced in many sections of this book. This situation is more complex than the configuration studied by Mittal. A rigid mass that is supported by an ideal spring and that is not subject to any damping shows only one single oscillation frequency. Here we study the interaction to a two dimensional elastic beam. This solid problem itself is more complex, the oscillation of the beam shows several modes in horizontal and vertical direction. Considering the coupling to a rigid body, the fluid forces act as averages on the center of mass and all possible motions of the solid can be described by a two dimensional vector. The elastic case asks for modeling of a distributed deformation vector in the two dimensional solid domain. Fluid's forces not necessarily cause a motion of the solid, they also give rise to bending and compression.

In the following section we first describe the coupled fluid-structure interaction test case. Then in Sect. 11.2, we discuss the solid problem without a surrounding fluid. In Sect. 11.3 we consider the fluid flow around a rigid obstacle and finally in Sect. 11.4 we analyze the coupling.

11.1 Configuration of the Test Case

The configuration of the benchmark problem is shown in Fig. 11.1a. The original *fsi-3* benchmark problem published by Hron and Turek [200] used the average inflow velocity $\bar{\mathbf{v}} = 2\,\mathrm{m}\cdot\mathrm{s}^{-1}$. This choice of parameters results in the Reynolds number

$$Re = \frac{\bar{\mathbf{v}}D}{\nu} = \frac{2\cdot 0.1}{0.001} = 200,$$

where $D = 0.1\,\mathrm{m}$ is the diameter of the circle, the rigid part of the obstacle. The attached elastic beam is not considered for computing the Reynolds number. In Fig. 11.1b we show the deflection in $A = (0.6, 0.2)$, a point in the tip of the beam, for these settings. The coupled dynamics results in a periodic oscillation with dominant frequency

$$f_{\bar{\mathbf{v}}=2} \approx \frac{1}{0.184} \approx 5.435. \tag{11.2}$$

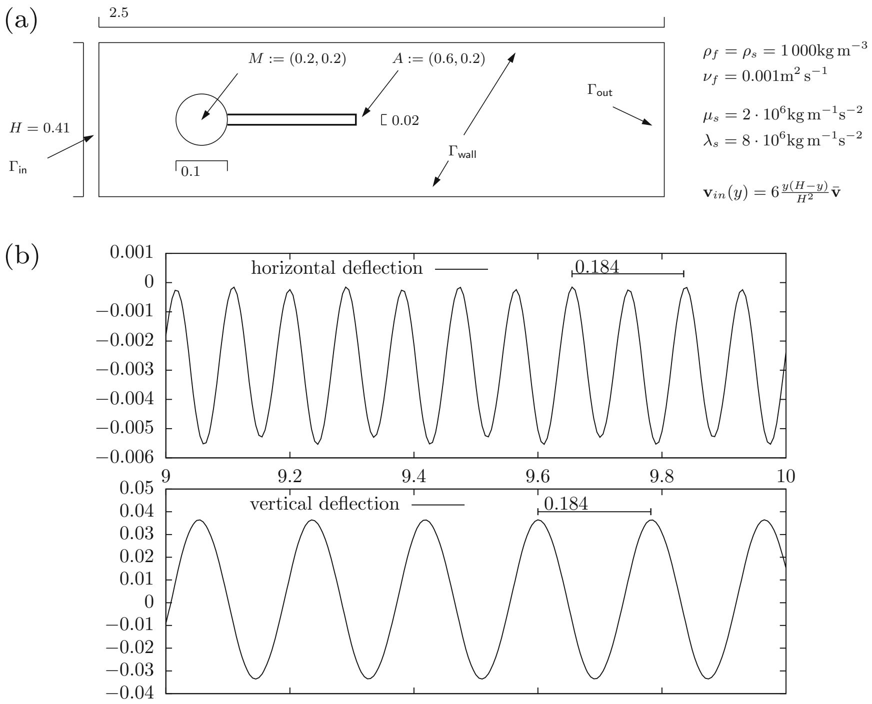

Fig. 11.1 We show the configuration of the benchmark problem as well as the dominant oscillation in the beam's tip. (**a**) Configuration of the fluid-structure interaction problem*fsi-3*. (**b**) Horizontal and vertical deflection $\mathbf{u}_x(A)$, $\mathbf{u}_y(A)$ in the tip of the beam $A = (0.6, 0.2)$

Considering the horizontal and vertical deflection of the tip of the beam, twice the amplitude of the oscillation is given by

$$2a^x_{\bar{\mathbf{v}}=2} \approx 0.00538, \quad 2a^y_{\bar{\mathbf{v}}=2} \approx 0.0701,$$

measures as the distance between maximal and minimal deflection. In Sect. 5.1.1 we have studied the discrete Fourier transform of the drag coefficient. Here we have found high frequent oscillations that superimpose the dominant frequency. While not visible at a first sight their numerical resolution is necessary to obtain the correct dynamics of the coupled system.

11.2 Dynamics of the Elastic Solid

To identify the dynamics of the isolated elastic structure we run preliminary tests without the fluid problem. These computations are comparable to the *csm-3* benchmark case published by Hron and Turek [200]. We initially expose the beam to a vertical force

$$\mathbf{f}_s(t) = \begin{pmatrix} 0 \\ -1 \end{pmatrix} \cdot \begin{cases} 10\rho_s & t \le 0.05\,\text{s} \\ 0 & t > 0.05\,\text{s}. \end{cases}$$

The resulting oscillation of the beam's tip is shown in Fig. 11.2. The time interval $I = [8, 10]$ is chosen such that the dominant frequencies are visible. The beam is not oscillating with one single frequency but it shows a superposition of many different frequencies. We can however identify the dominant frequency (of the vertical deflection) as

$$f_s \approx \frac{1}{0.464} \approx 2.155,$$

which is about half of the *fsi-3* frequency $f_{\bar{\mathbf{v}}=2}$ given in (11.2). Naturally, the horizontal deflection shows twice of the frequency, as the tip is deformed to the left two times in every cycle. The oscillations shown in Fig. 11.2a are far from a sine wave. Therefore we show in the lower part of Fig. 11.2b the discrete Fourier transformation of the periodic dynamics. First, one clearly identifies the dominant frequencies of the horizontal and vertical deflections, where the horizontal one is twice as large as the vertical one. In addition we observe oscillations at higher frequencies that explain the complex structure of the periodic solution.

In contrast to the test case studied by Mittal [245, 250, 260], the situation is less clear. If we want to show synchronization effects it is not obvious, if this will appear at the most dominant frequency or at an overtone.

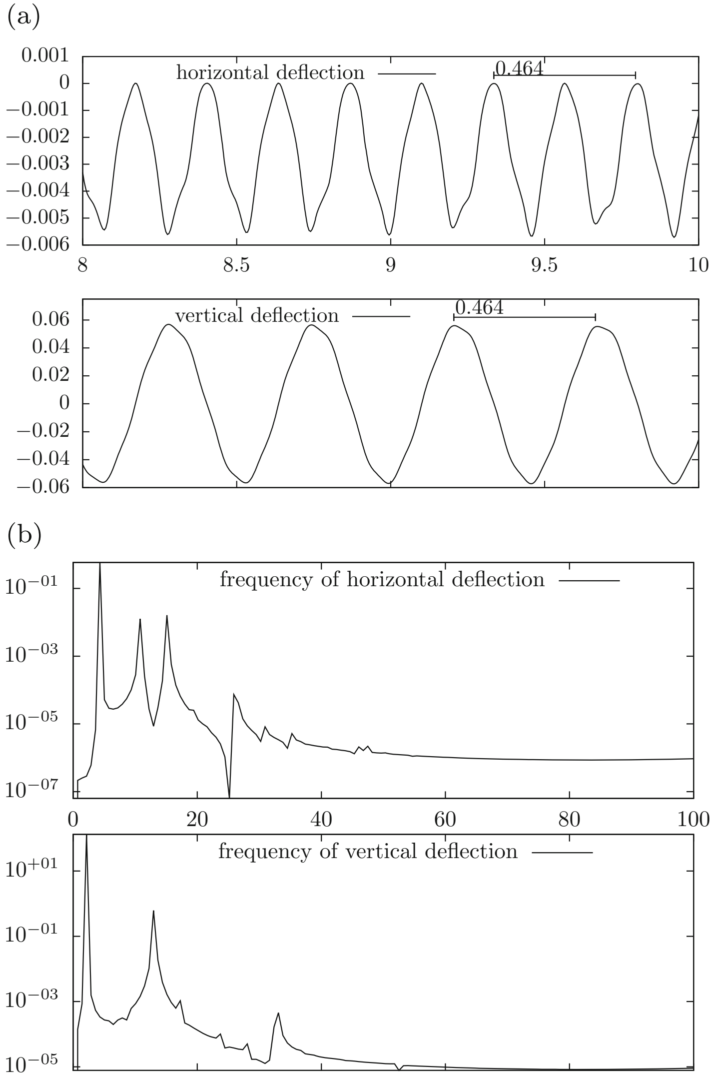

Fig. 11.2 Dynamics of the solid problem. The dominant Eigenfrequency for the horizontal deflection is $f \approx 4.3$ the vertical one is $f \approx 2.15$. (**a**) Deflection of the tip of the beam $A = (0.6, 0.2)$ in the temporal interval $I = [8, 10]$. (**b**) Discrete Fourier components of the beam's deflection. We indicate the strength of the signal for the different frequencies

11.3 Dynamics of the Flow Around a Fixed Obstacle

Next, we study the pure fluid-dynamics test case, where the obstacle is considered to be rigid. Of coarse, there will be no deflection. Instead we measure the *drag* and *lift coefficient* of the obstacles that should show a similar dynamic behavior.

For increasing average inflow velocity $\bar{\mathbf{v}}$ (which corresponds to increasing Reynolds numbers) we note the frequency of the vortex street. For easy measurement, we consider the forces of the fluid on the obstacle in cross-direction, measured as

$$F_y = -\int_{\mathcal{I}} \boldsymbol{\sigma}_f \mathbf{n} \cdot \mathbf{e}_y \mathrm{d}o,$$

where $\mathbf{e}_y = (0, 1)^T$. Up to a scaling, this function corresponds to the lift coefficient. We indicate frequency f_y and amplitude a_y for the functional in Table 11.1. The flow develops a periodic oscillation at $Re \approx 170$. We once more note that we did not include the beam into the definition of the Reynolds numbers. This is the reason for the rather high value of $Re \approx 170$ for the transition to the laminar periodic state in contrast to $Re \approx 50$ for the flow around a circular obstacle only. In Fig. 11.3 we show the pressure profile for the flow at different Reynolds numbers.

Table 11.1 Frequency and amplitude of the vertical force on the obstacle (ball & fixed beam) for increasing Reynolds numbers

$\bar{\mathbf{v}}$	1.4	1.5	1.6	1.7	1.8	1.9	2.0	2.1	2.2	2.3	2.4	2.5	2.6	2.7	2.8	2.9
Re	140	150	160	170	180	190	200	210	220	230	240	250	260	270	280	290
f_y	–	–	–	3.62	3.85	4.04	4.22	4.42	4.63	4.82	5.04	5.21	5.43	5.63	5.85	6.06
$2a_y$	–	–	–	<1	9.88	111	154	197	240	283	323	371	420	469	521	565

Fig. 11.3 Pressure profile for the flow around a fixed obstacle at different Reynolds numbers. *From top to bottom*: $Re = 100, 200, 300$

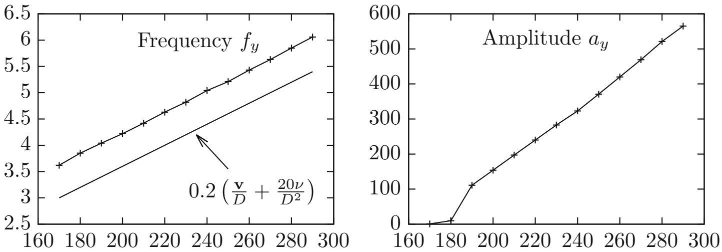

Fig. 11.4 Frequency and amplitude of the von Kármán vortex street for the flow around a fixed obstacle at different Reynolds numbers. The theoretical prediction for the frequency shows very good agreement (up to a constant shift)

Next, we compare the theoretical model for the oscillation frequency (11.1) with the numerical results. In Fig. 11.4, we show frequency and amplitude of the oscillation for different Reynolds numbers. Equation (11.1) predicts the slope of the frequency but gives a shifted curve. This is no contraction to theory, as our setting includes the fixed beam and is therefore more complex. We see that amplitude and frequency of the oscillation increase with the Reynolds number. For the frequency we derive the relation

$$f_y(Re) \approx 0.02Re + 0.24. \tag{11.3}$$

The amplitude also linearly depends on the Reynolds number and can be approximated as

$$2a_y(Re) \approx 4.5Re - 750. \tag{11.4}$$

Both relations are good approximations for $Re \in [180, 300]$.

11.4 Coupled Dynamics

Finally, we study the oscillation dynamics of the fully coupled fsi-3 fluid-structure interaction problem for different Reynolds numbers. Here we are interested in the interplay of von Kármán vortex sheet and structural oscillation. We start by showing snapshots of the solution for different Reynolds numbers starting in the stationary regime at $Re = 100$, see Fig. 11.5.

We also show the deformation of the beam. At low Reynolds numbers, the flow is stationary. Transition to a non-stationary oscillatory flow with large amplitudes is given for $Re \approx 135$ in contrast to $Re \approx 170$ for the pure fluid case. A closer look at the results even shows transition to non-stationary pattern (although at low amplitudes) for Reynolds numbers $Re \approx 115$.

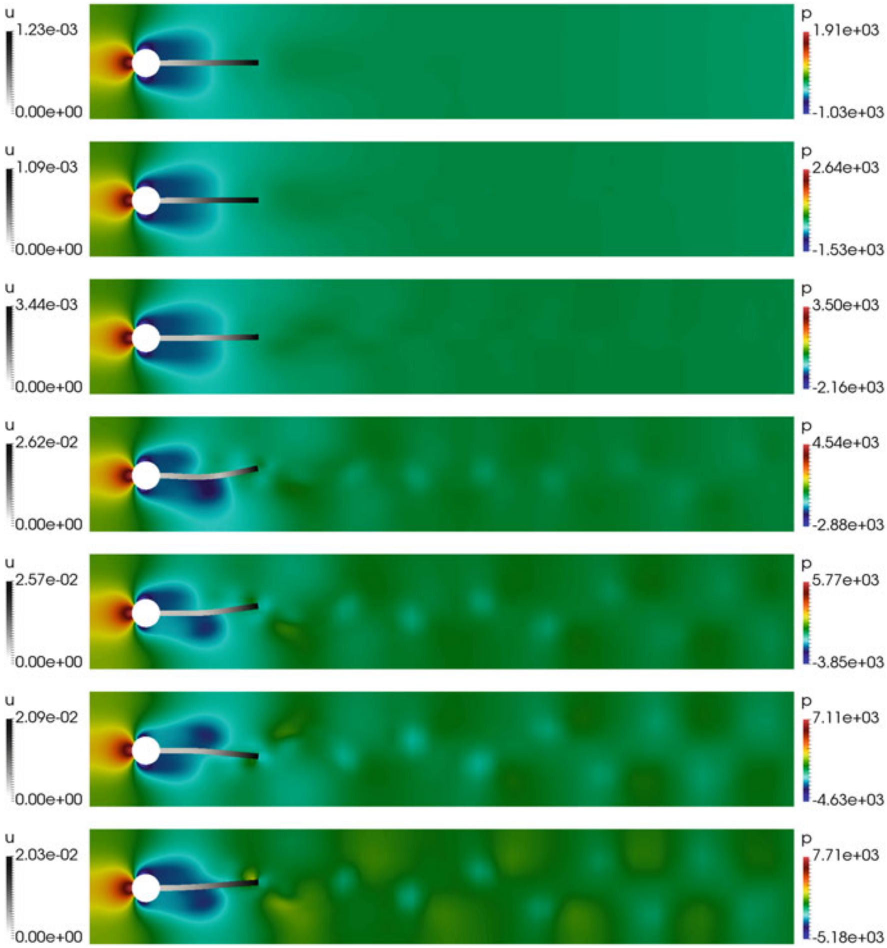

Fig. 11.5 Pressure profile for the flow and deformation $|\mathbf{u}_s|$ for the flow around an obstacle with elastic beam at different Reynolds numbers ranging from $Re = 100$ (*top*) to $Re = 200$ (every 20) and for $Re = 210$ (*bottom*)

In Table 11.2 we show the dominant frequency f_y and twice the amplitude $2a_y$ of the vertical deflection of the beam. Comparing to Table 11.1 we identify various differences. We also give a graphical representation of the findings in Fig. 11.6.

- A fully developed stable periodic solution is developed at $Re \approx 115$ compared to $Re \approx 170$ in the case with a fixed obstacle. For $115 \leq Re \leq 130$ there are however no significant forces on the obstacle. The deformation of the beam is very small such as the amplitude of the vertical force f_y.

Table 11.2 Frequency and amplitude of the vertical force for the coupled fluid-structure interaction problem at different Reynolds numbers

$\bar{\mathbf{v}}$	1.1	1.15	1.2	1.25	1.3	1.35	1.4	1.5	1.6	1.7	1.8	1.9	2.0	2.1	2.2	2.25	2.3
Re	110	115	120	125	130	135	140	150	160	170	180	190	200	210	220	225	230
f_y	4.82	4.97	5.10	5.19	5.40	5.52	4.09	4.34	4.57	4.79	5.00	5.26	5.48	5.71	5.95	14.8	14.9
$2a_y$	$\ll 1$	58	142	141	130	104	206	300	345	364	376	375	361	348	334	1020	1266

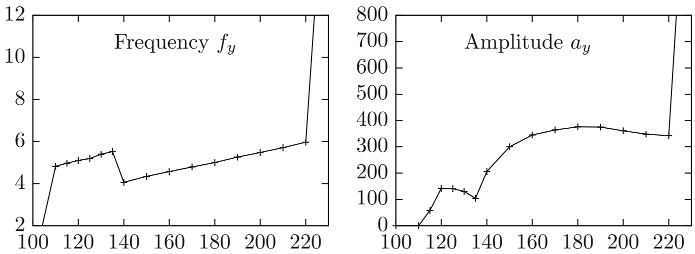

Fig. 11.6 Frequency and amplitude for the coupled fluid-structure interaction problem

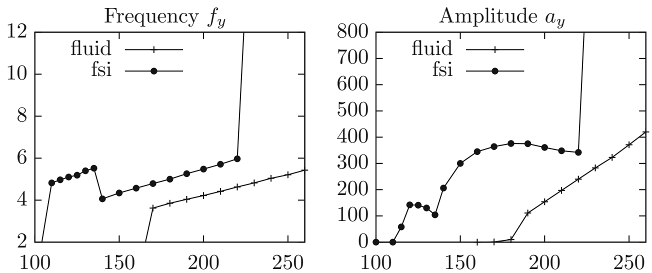

Fig. 11.7 Comparison of frequencies and amplitude for the fluid problem and the coupled fsi problem

- Starting with $Re \approx 135$ a stable periodic solution with significant amplitude and large deformations of the beam develops. This regime is stable up to $Re \approx 220$. For larger values of the Reynolds number the non-stationary dynamics are more complex with dominant overtones and rapidly increasing amplitude.
- The frequency of the oscillation increases with the Reynolds number. There is however a significant jump at $Re \approx 130{\sim}135$ where an oscillation with large amplitude appears. The slope of the frequency development $f_y(Re)$ is nearly the same as in the fluid case given in (11.3). We show a direct comparison of the two frequencies in Fig. 11.7.
- For the fluid problem the amplitude was linearly depending on the Reynolds number (11.4). The coupling to the solid has a stabilizing effect on the amplitude. For a large interval $Re \in (150, 220)$ the amplitude takes values of $2a_y \approx 375$. The direct comparison is given in Fig. 11.7.

From this numerical study, we cannot derive any analytical relation between the frequencies of the von Kármán vortex sheet, the Eigenfrequency of the solid and the frequency of the coupled dynamics. It is obvious that the elastic solid has a destabilizing effect. Relating to the discussion on the *added mass effect* given in Sect. 3.3 we have to expect this effect. Non-stationarities appear at lower Reynolds numbers.

As Mittal and coworkers [245] we could identify a sub-critical regime $Re \in (110, 170)$ where the pure fluid problem is stationary but a coupling to an elastic solid gives stable oscillatory solutions.

Mittal and coworkers [245, 260] found a synchronization regime for the frequency of the vortex shedding and the frequency of the solid's oscillation for a large range of Reynolds numbers. We could not identify such a synchronization for the elastic fluid-structure interaction problem in Fig. 11.6. No immediate relation between the frequencies of the coupled fluid-structure interaction problem and the structural frequency is observed. Instead, we get a linear dependency between frequency and Reynolds number with exception of a jump at the critical value $Re \approx 130{\sim}135$ where dynamics with a substantial amplitude developed.

However we see a strong stabilizing effect in the amplitude of the oscillation, compare Fig. 11.7. For the complete range of Reynolds numbers $Re \in (130, 210)$ we observe amplitudes $2a_y \approx 375$ that do not grow with increasing inflow velocities.

In Fig. 11.8 we show the oscillation of the vertical force plotted over time. We always show a time interval (each of them has the length 2 s where the flow reached a stable periodic state. We show the situation at $Re \approx 110 \sim 120$ where the transition to an periodic oscillation with an amplitude of $2a_y \approx 150$ is initiated. This regime is stable for $Re \in [120, 135]$. Here, larger Reynolds numbers will lead to higher frequencies but smaller amplitudes. Next, we show the transition at $Re \approx 135 \sim 140$, where we experience the jump to a lower frequency, but where the amplitude is increased to about $2a_y \approx 300$. This regime is stable for $Re \in [140, 220]$ showing an increase in frequency and more or less stable amplitudes for larger Reynolds numbers. Only in the transition zone for $Re \approx 140$ the functional pattern in Fig. 11.8b (right) shows a visible second mode. Finally we show the next transition at $Re \approx 220 \sim 225$ to a more complex flow pattern. Both the frequency and amplitude are strongly intensified. For even larger Reynolds numbers the computations will break down due to very large oscillations and instabilities of the ALE formulation.

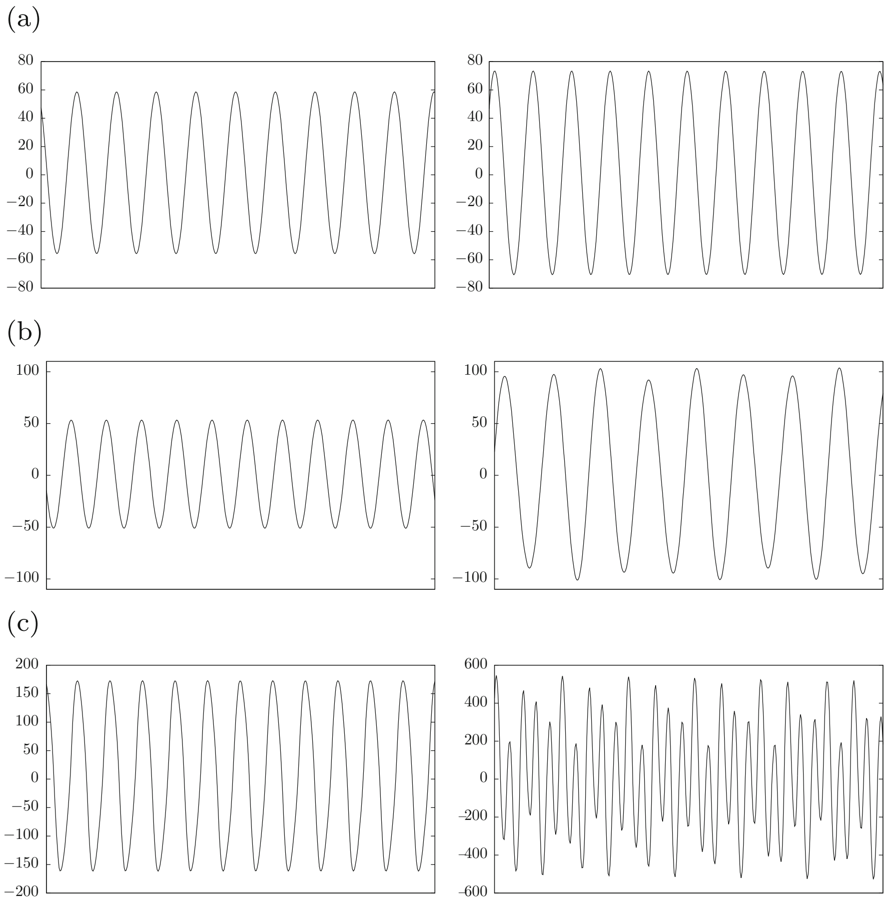

Fig. 11.8 Dynamics of the vertical force of the coupled fluid-structure interaction problem for different Reynolds numbers. We show the formation of the stable oscillation with large frequency and small amplitude at $Re \approx 115$ (**a**), the transition to a stable oscillation with smaller amplitude $Re \approx 135$ (**b**) and the transition to an unstable oscillation at $Re \approx 225$ (**c**). Note the different scaling on the vertical axis in the bottom row. On the horizontal axis we always show an interval of 2 s. (**a**) $Re = 115$ and $Re = 120$, (**b**) $Re = 135$ and $Re = 140$, (**c**) $Re = 220$ and $Re = 225$